universität innsbruck

Gaussian beams

Alexander Helbok[*], Jakob Höck [†], Max Koppelstätter[‡]

April 15, 2024

Abstract

The aim of this report is to characterize Gaussian beams. Firstly, the beam diameter of the laser is recorded at different distances with and without a lens, allowing us to determine the beam waist by comparing with theory. We determine the beam waist to be $W_0 = 224(4)$ µm. The second part of the experiment includes an optical cavity, allowing us to study higher modes of the laser. We can qualitatively identify TEM_{01}, TEM_{10} and TEM_{02} modes using a CCD camera. We also recorded a spectrum of higher order modes and determined the frequency separation. We can explain the measured mode spacing by assuming contributions to the spectrum coming exclusively from TEM_{mn} modes with $m + n = 2$.

[*]alexander.helbok@student.uibk.ac.at
[†]jakob.hoeck@student.uibk.ac.at
[‡]max.koppelstaetter@student.uibk.ac.at

Contents

0 Introduction

What would a world without laser technology look like? Well, it would look really different from the world we know. From GPS to accurate clocks, lasers are omnipresent in the modern world. But not only technical applications are worth mentioning here; they also play an indispensable role in various physical experiments, shedding light on phenomena ranging from quantum mechanics to material science. In this experiment, we focused on the laser beam's characteristics and its coupling to an optical cavity.

In this analysis, our focus is twofold. Firstly, we investigated the propagation behavior of the laser beam. We did this by measuring the beam's diameter at various distances and comparing with theoretical predictions. Secondly, we focused on the mode behavior of a cavity. To accomplish this, we had to align the laser's mode to the one of the cavity, using a lens. Finally, we deliberately misaligned the beam to get a view of higher order modes of the beam. A CCD camera was used to optically capture these, whilst the spectrum was recorded on an oscilloscope via a photodiode.

Following a brief theoretical overview and an explanation of the applied theory, this report will present and discuss the evaluated data.

1 Theory

In this section, the basic theoretical principles are briefly outlined to provide a better understanding of what a Gaussian beam is and how a cavity works.

1.1 Gaussian beam

The Gaussian modes are a set of solutions to the Helmholtz equation, which can be derived from Maxwell's equations using the paraxial approximation (see [1]). Their intensity is given by

$$I(x,y,z) \sim |U(x,y,z)|^2 = I_0 \left(\frac{w_0}{w(z)}\right)^2 \cdot \exp\left(-2\frac{x^2+y^2}{w(z)^2}\right),$$

where w_0 is the beam radius when in focus (also known as the beam waist), $w(z)$ is the radius of the beam at a given location z, I_0 is the original intensity of the laser and y is the spacial expansion. The beam width is given by

$$w(z) = w_0\sqrt{1+\left(\frac{z}{z_R}\right)^2}. \tag{1}$$

Here $z_R = \pi \cdot w_0/\lambda$ is called the Rayleigh length, which is given by the distance at which the intensity decreases by the factor $1/e^2$, at this point the beam width increases by $\sqrt{2}$. Via geometrical analysis, expressions for the curvature of the beam $R(z)$ and the divergence angle θ can be found (see [1]).

The Rayleigh length divides the beam into two regimes, a near field, where the beam can be regarded as a plane wave (curvature $R = \infty$) and far field, where the beam can be regarded as a ~~cubic~~ wave ($R(z) \sim z$).

1.2 Matrix formalism

In order to describe the effect of optical elements on a Gaussian beam, the ABCD matrix formalism can be used. Therefore, we define a complex quantity $q(z)$, such that

$$\frac{1}{q(z)} = \frac{1}{R(z)} - i\frac{\lambda}{\pi w(z)^2}.$$

When passing an optical element, the complex quantity changes according to

$$\frac{1}{q_2} = \frac{C + D/q_1}{A + B/q_1}.$$

The parameters A,B,C, and D are entries of a 2×2 matrix. The form of the matrices for free propagation, lenses and mirrors are given in Figure 1. Combination of optical elements is done via matrix multiplication, where the multiplication order corresponds to the order of propagation.

Optical element	$\begin{pmatrix} A & B \\ C & D \end{pmatrix}$ Matrix
Free propagation for distance d	$\begin{pmatrix} 1 & d \\ 0 & 1 \end{pmatrix}$
Lens with focal length f	$\begin{pmatrix} 1 & 0 \\ -\frac{1}{f} & 1 \end{pmatrix}$
Mirror with radius of curvature r	$\begin{pmatrix} 1 & 0 \\ -\frac{2}{r} & 1 \end{pmatrix}$

Figure 1: Matrix entries for lenses, mirrors and free propagation in space. Table taken from [1].

Using this formalism, we can calculate the beam waist w_2 of an incident collimated beam with waist w_1 and curvature $R = \infty$ at a distance $z = f$ after passing through a lens with focal length f. The result

$$w_2 = \sqrt{\frac{f^2 w_1^2 \lambda^2}{\pi^2 w_1^4 + f^2 \lambda^2}} \approx \frac{f\lambda}{\pi w_1} \tag{2}$$

can be further simplified, assuming $f^2\lambda^2$ to be negligibly small.

1.3 Optical Resonator

In an optical resonator, two mirrors are set up parallel to each other at a certain distance L. Due to the fact that the electric field has a node at each mirror, only waves with a wavelength λ that is an integer inverse of the half distance between those mirrors can exist as standing waves. So we get the general relation

$$\lambda_n = \frac{2L}{n},$$

where n is an integer. Changing wavelength to frequency ν and introducing the free spectral range (FSR) as $\Delta\nu_{\mathrm{FSR}} = c/2L$ the relation can be simplified to $\nu = n\Delta\nu_{\mathrm{FSR}}$ (see [2]). If the mirrors are semi-transparent, monochromatic light can be transmitted. Depending on the

reflectivity, other frequencies can also pass through the mirror and the peaks smooth out [3].

To quantify the quality of a cavity, we introduce the finesse $\mathcal{F}$ of a cavity, defined as the ratio between the FSR and full width at half minimum (FWHM) of the transmitted peaks. Assuming all losses coming from mirror transmission, we can theoretically compute the finesse. Both relations are listed below

$$\mathcal{F}_{\text{exp}} = \frac{\Delta\nu_{\text{FSR}}}{\text{FWHM}} \qquad \mathcal{F}_{\text{theo}} = \frac{\pi\sqrt{R}}{1-R}, \tag{3}$$

with R being the mirror reflectivity.

A confocal resonator has a special geometry, where both mirrors are curved with the same radius r as the length L between them ($r = L$). This has some essential benefits, such as the fact that when correctly aligned the stability is very high. Additionally, if the laser beam is misaligned, we only get one peak between the two expected beams (see [4]) .

A resonator decomposes an incident laser beam into its internal modes. To achieve maximum spatial overlap of laser and resonator mode, the laser mode has to be adjusted using lenses. To calculate the needed beam waist, we use

$$2z_{\text{R}} = \frac{2\pi w_0}{\lambda} = \sqrt{L(2r-L)}. \tag{4}$$

Here, a confocal resonator is used with equal mirror curvatures r.

If the laser and cavity modes do not match, apart from the fundamental transverse electromagnetic mode (the TEM_{00}), also higher modes (TEM_{mn} with $m, n > 0$) are excited. These excited states can be constructed by multiplying the ground state with Hermite-polynomials H_i, resulting in so called Hermite-Gaussian-beams:

$$U_{(\text{m,n})} \sim U_{(0,0)} H_{\text{m}}\left(\frac{\sqrt{2}}{w(z)}x\right) H_{\text{n}}\left(\frac{\sqrt{2}}{w(z)}y\right). \tag{5}$$

Each revolution in the cavity gives the modes an additional phase shift, which changes the resonance condition from $\nu = n\Delta\nu_{\text{FSR}}$ to

$$\nu_{q,m,n} = \left[(q+1) + \frac{1}{\pi}(m+n+1)\arccos\left(1-\frac{L}{r}\right)\right]\Delta\nu_{\text{FSR}}. \tag{6}$$

In case of a confocal resonator ($r = L$) the relation simplifies to

$$\nu_{q,m,n} = \left[(q+1) + \frac{1}{2}(m+n+1)\right]\Delta\nu_{\text{FSR}}. \tag{7}$$

This leads to half-axial-modes of a confocal resonator, as shown in the spectrum of a near planar, a confocal and a near concentric cavity in Figure 2.

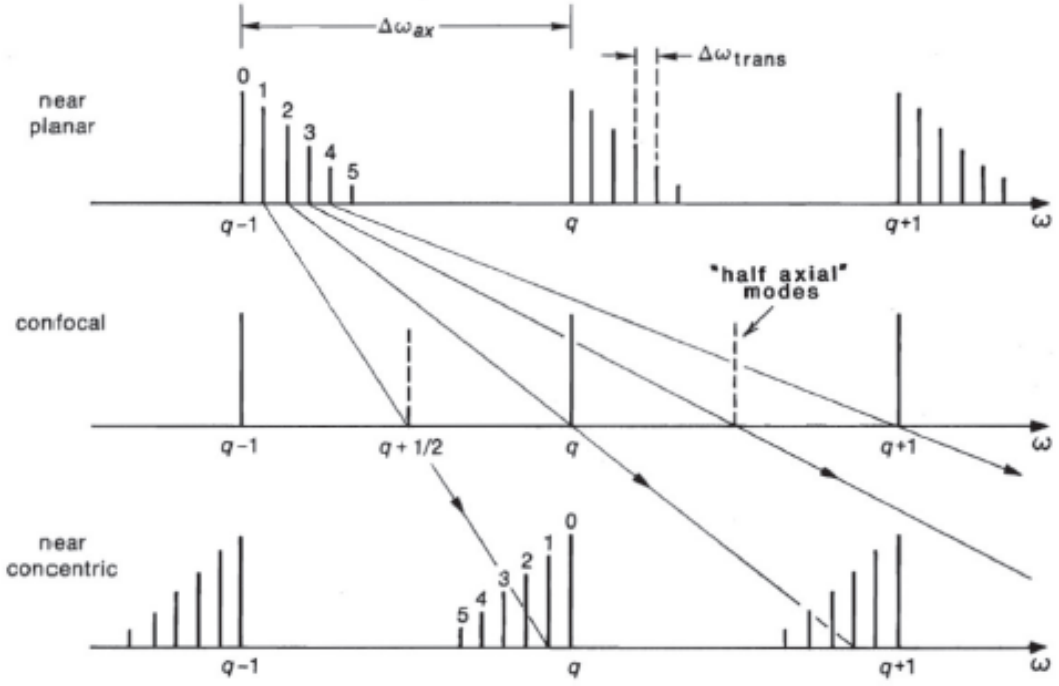

Figure 2: "Resonance frequencies of higher order modes in optical resonators for different configurations. "[1] Figure taken from [1].

2 Procedure and Setup

The experiments begin with a characterization of the Gaussian beam. Afterward, modes of the laser in a cavity are analyzed.

2.1 Beam profiling

The first step is to determine the width of the waist of the beam emitted by a HeNe laser with a wavelength of $\lambda = 633$ nm. After the laser, a Faraday isolator (FI) is placed, which protects the laser from back reflections.

The beam width is measured at various distances from the laser. In total 11 measurements are taken in steps of 1.5 cm, starting closely after the FI. The beam width was measured using a waistmeter, which contatins a photodiode measuring the intensity, and a rotating disc. This rotating disc alternately covers the photodiode so that the width of the beam can be determined if the disc's rotation speed and geometry are known. Since the waistmeter indicates the actual diameter, it must later be halved to obtain the radius of the beam.

After these measurements, a lens with a focal length of $f = 100$ mm is placed after the Faraday isolator. The same procedure is then repeated.

2.2 Mode matching

In preparation for the experiment, the beam waist of the cavity was determined. This can be done using Equation (4) and $r = L = 150$ mm and we get $w_0 = 122.93$ µm.

The next step is to match the resonator waist to the beam waist of the laser using a suitable lens. In Figure 3 the simulated beam with a lens is shown, which is used to determine the best focal length of the lens we want to use for the following steps. In the simulation, the result for the beam diameter and the divergence angle from the first part of the experiment is used.

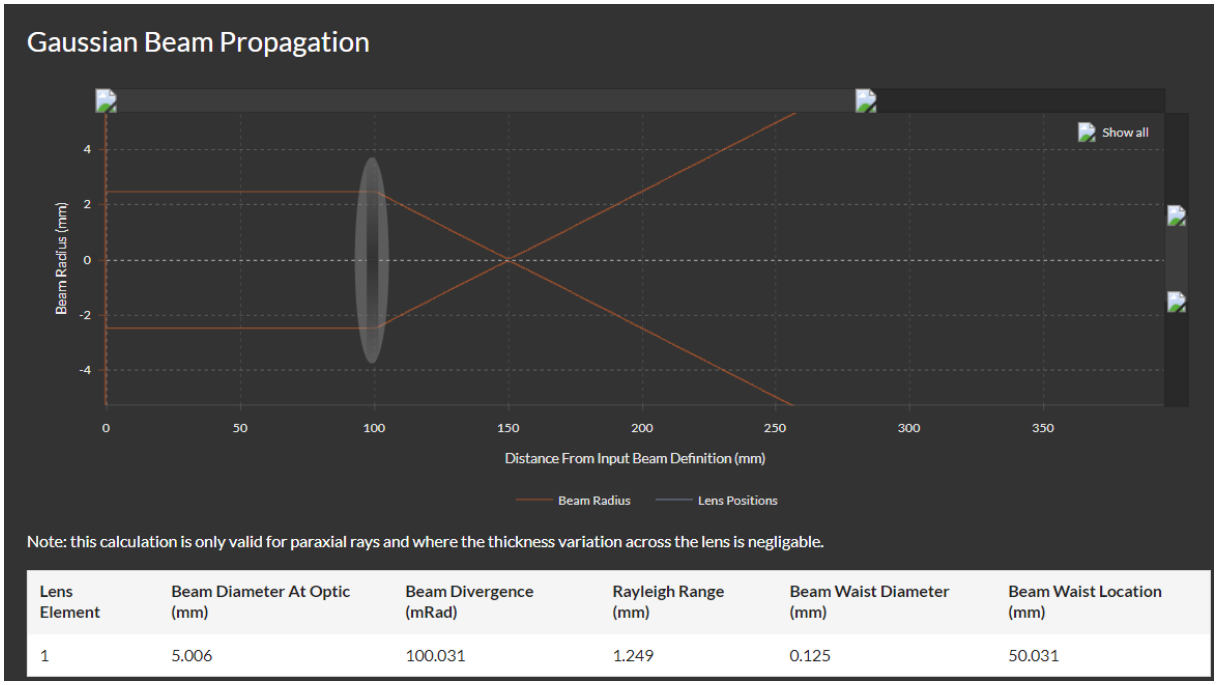

Lens Element	Beam Diameter At Optic (mm)	Beam Divergence (mRad)	Rayleigh Range (mm)	Beam Waist Diameter (mm)	Beam Waist Location (mm)
1	5.006	100.031	1.249	0.125	50.031

Figure 3: Simulation for a Gaussian beam with a beam waist diameter of 0.44 mm and a full angle beam divergence of 1.83 mRad, including a lens with focal length 200 mm, placed at 550 mm from the beam focus. Simulation made with [5].

It turns out that 200 mm yields the results. Once the lens is in place, the next step is to align it correctly, then adjust the subsequent mirrors and the cavity mirrors to ensure that the laser beam is in a straight line. This entire structure can be seen in Figure 4.

After the laser beam leaves the Faraday isolator it passes through a lens and is redirected by two mirrors. It then enters a cavity consisting of two mirrors, one of which is placed on a movable mount, whilst the other is mounted onto a Piezo-transducer, connected to a function generator. This enables us to minimally change the cavities length, effectively scanning frequencies. After the latter cavity mirror, the laser beam passes a beam splitter, directing one part onto a CCD-camera, which is used to take pictures of the incoming beam, while the other part is directed onto a photodiode, connected to an oscilloscope.

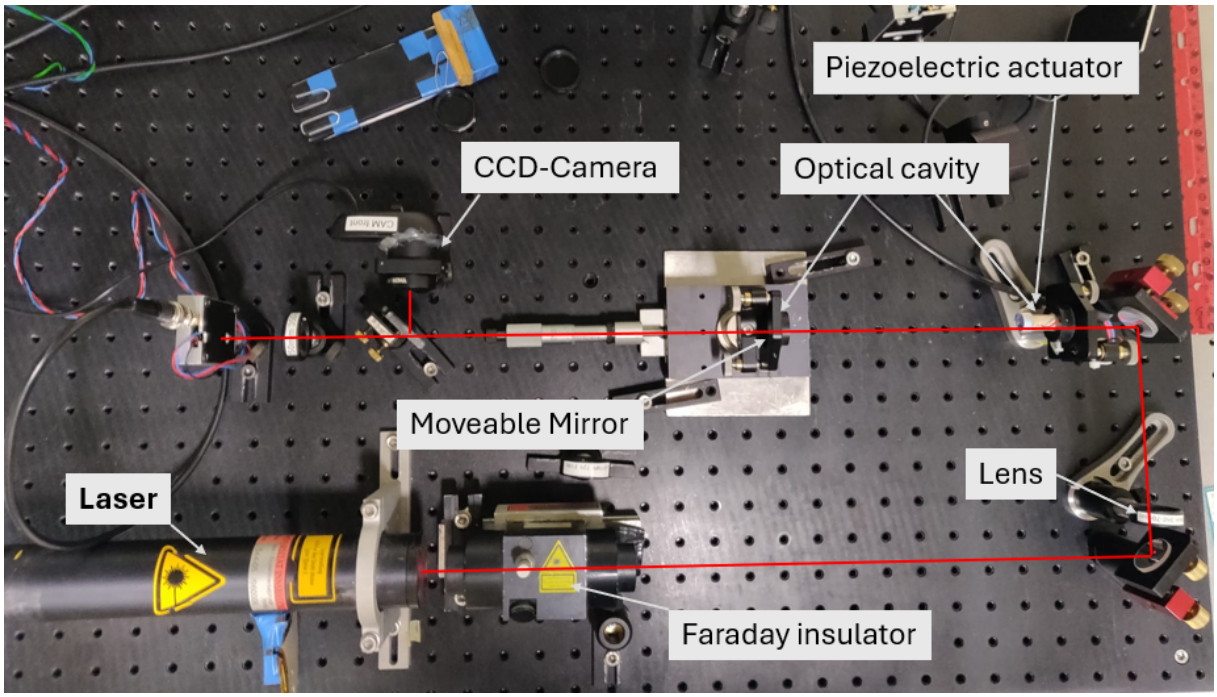

Figure 4: The entire setup from the laser to the photodiode and the CCD camera is visible via the Faraday isolator, built-in lens, and optical cavity, which includes a piezoelectric actuator and an adjustable mirror. A beam splitter allows simultaneous irradiation of the two objects. The Faraday isolator ensures that the reflected beam does not return to the laser.

2.3 Study of cavity modes

The resonator is first visually aligned by overlapping the mirror reflections and then fine tuned using the output on the oscilloscope maximizing the transmission of the TEM_{00} mode. Here we recorded two spectra, one with perfect alignment to study the transmission and the other one with slightly misaligned mirrors to measure the distance to half axial modes.

After this, the length of the resonator was increased by 13.53(1) mm using the adjustable mirror to make higher modes visible. In a confocal resonator, these are always projected between two intensity peaks (see subsection 1.3). One of the deflection mirrors was then adjusted so that the laser no longer falls directly into the resonator. This allows higher modes to be detected on the photodiode, as well as the CCD camera. It is important to note that any change in resonator or laser alignment can affect the visible modes, so careful calibration and control is required throughout the process. The oscilloscope readings and images from the CCD camera are stored for later analysis.

3 Results

We start by analyzing the lasers beam parameters by recording the beams radius w at different distances z. The latter was measured using a millimeter-scale ruler with chosen uncertainty of 1 mm. Due to some fluctuations in the waistmeter's reading, we chose the uncertainty to be 3 µm, which could be reduced by taking multiple readings and averaging. 11 datapoints were taken in steps of 1.5 cm and can be seen in Figure 5. Additionally, a function following

Equation (1) was fitted and can be seen as solid orange line, accompanied by a 1σ confidence band.

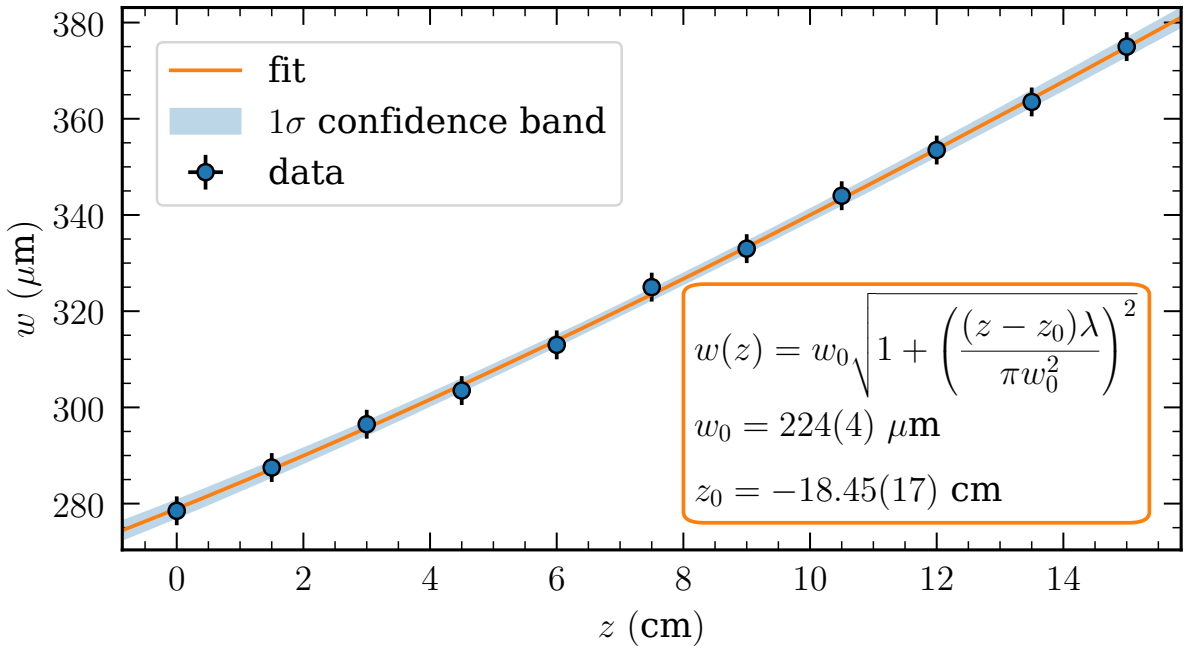

Figure 5: The measured beam radius w of freely propagating laser light is plotted against the distance z. A function was fitted and can be seen as orange line and is surrounded by a 1σ confidence band. The fitfunction and according parameters can be seen in the bottom right. Errorbars denote 1σ uncertainties with the errors in x-direction being too small to make out.

In Figure 5, we can see that the data nicely follows theory (all datapoints are within 1σ of the fitted curve). We can extract a beam waist $w_0 = 224(4)$ µm at a focus position of $z_0 = -18.45(17)$ mm, which approximately lies at the end of the laser housing.

Before using the determined beam waist to match it to a cavity, we analyzed the effect of a lens with focal length $f = 100$ mm on the beam radius. Again, data was taken in intervals of 1.5 cm with the same uncertainties as described above. The data with an appropriate fit can be seen in Figure 6. Here a 2σ confidence band was chosen, to help gauge the deviation of the datapoints from the fit line around the focus point.

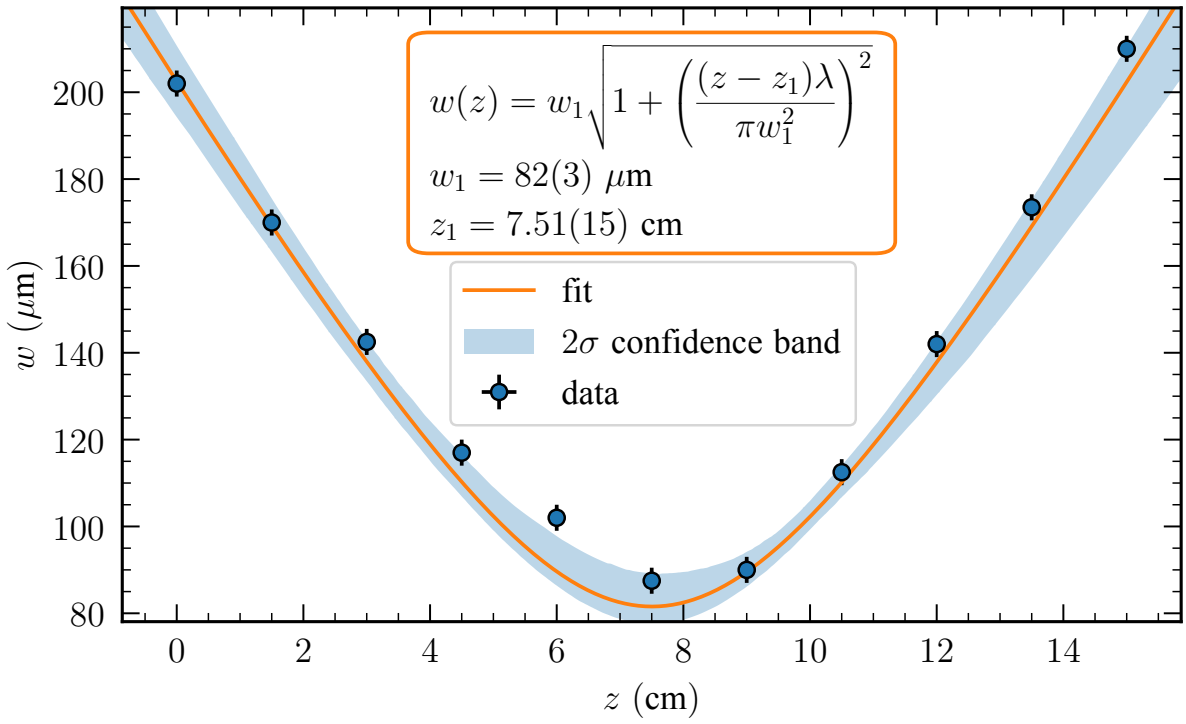

Figure 6: The measured beam radius w of laser light after a lens with $f = 100$ mm is plotted against the distance z. A function was fitted and can be seen as orange line and is surrounded by a 2σ confidence band. The fitfunction and according parameters can be seen in the upper middle. Errorbars denote 1σ uncertainties with the errors in x-direction being too small to make out.

The data in Figure 6 mostly follows the expected behavior, with outliers around the focus point $z_1 = 7.51(15)$ cm. This could have been caused by the waistmeter being slightly tilted against the laser's propagation axis, leading to higher radius measurements. After adding the distance between the closest radius measurement and the lens, which was estimated to be 2.5(2) cm, $f_{\text{exp}} = 100(2)$ mm is in good agreeance with $f_{\text{lens}} = 100$ mm. As for the waist, using the matrix formalism described in subsection 1.2 we can get a theoretical prediction for the beam waist after a lens. Comparing the exact theoretical result with the experimental value

$$w_{1,\text{theo}} = 83.3(1.1)\ \mu\text{m} \qquad w_{1,\text{exp}} = 82(3)\ \mu\text{m},$$

we conclude that our experiment is consistent with theory. The approximating $w_1 = f\lambda/\pi w_0$ yields a value of 89.7(1.6) µm, which deviates significantly from both, experimental and exact theoretical result. It is therefore not appropriate to use this approximation on a lens with focal length $f = 100$ mm.

After matching the lasers beam waist to that of the cavity (for a detailed procedure see subsection 2.2), we can validate the confocal condition (mirror curvature r equal mirror distance L) by measuring the distance to half axial modes. For this the transmitted laser signal was recorded on the oscilloscope and normalized using the highest datapoint (normalization was done for convenience). Then we isolate the peaks intended for studying and we fit a multilorentzian function (sum of multiple Lorentz functions with independent parameters) to the data. By

calculating the free spectral range of the cavity $\nu_{\mathrm{FSR}} = c/2L = 1$ GHz and the fitted distance between peaks of the same height, we can convert the time domain measurement from the oscilloscope to frequencies. The fit also lets us compute the distance between "regular" and half axial modes. All this can be seen in Figure 7.

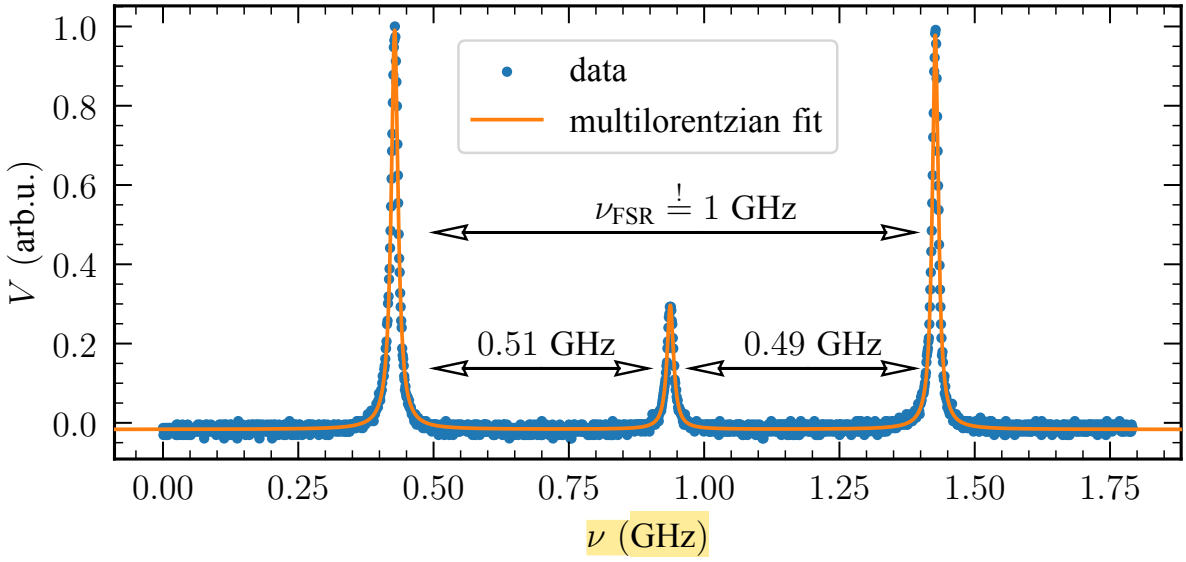

Figure 7: The recorded signal amplitude V is plotted against the frequency ν. A fit function consisting of three independent Lorentz functions was fitted and can be seen as solid line. The distance between the two TEM_{00} peaks was used to calibrate the x-Axis, while the distance to the half axial peak, seen in the middle was determined from fit parameters.

As can be seen in Figure 7, the confocal condition is almost met, with distances of 0.49 GHz and 0.51 GHz. Statistical errors are omitted, since the fit returned values in the range of kHz, at which systematical errors probably play a critical role.

Having confirmed the cavity to be confocal, we can optimize the mirrors to maximize the mode's intensity (by reducing the half axial mode's intensity). We then repeat the same procedure seen in Figure 7, with the only difference being that we recorded and fitted four Lorentz functions. We can evaluate the finesse $\mathcal{F}$ for each Lorentz peak using Equation (3) and the fitted full width at half minimum (FWHM). Assuming a mirror reflectivity of $R = 98\%$ and mirror transmission being the only losses, we can compute a theoretical upper limit for the finesse. Below are the theoretical limit and a mean of experimentally determined finesse values:

$$\mathcal{F}_{\mathrm{theo}} = 155.50 \qquad \mathcal{F}_{\mathrm{exp}} = 75.91(15)$$

It is apparent, that other loss mechanisms are at play in the system.

So far, we have only studied TEM_{00} and TEM_{01} modes. We can go to higher modes by increasing the cavity's length by 13.53(1) mm and exiting the confocal condition. We study higher modes qualitatively, by taking pictures with a CCD camera. The pictures are plotted in Figure 8. Additionally, we converted the images to grayscale and used it as proxy for the beam's intensity. This allows us, to project the image onto the horizontal and vertical axis by summing over the images rows and columns. We can fit Hermite-Gaussian functions of the appropriate

order to the projections. Both data (black) and fit (red) are plotted on the marginal axes in Figure 8.

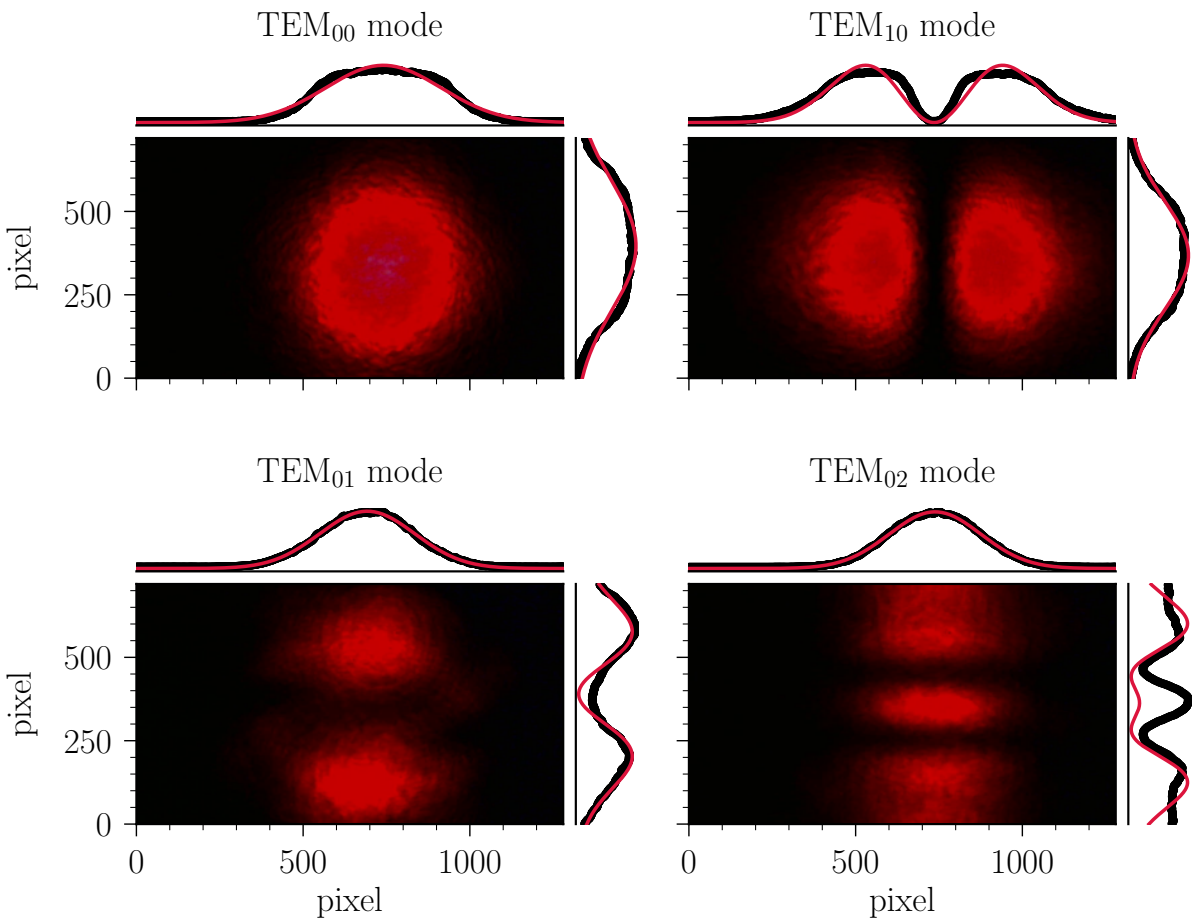

Figure 8: Four images of different TEM modes are depicted on a per-pixel basis. All of them are accompanied by marginal axes, onto which the intensity is projected and shown as black datapoints. The red lines represent fitted Hermite-Gaussian polynomials.

Looking at Figure 8, we can clearly identify TEM_{00}, TEM_{10} and TEM_{01} modes, with projected intensities matching the fitted Hermite-Gaussian function. The TEM_{02} mode (or possibly higher) is vertically not completely captured by the CCD camera, which makes fitting to difficult. In the top two pictures we saturate the CCD's recordable brightness. This can be directly observed in the optical picture as color discontinuity towards the center of the laser beam, further supported by a plateauing off toward the maximal intensity in all marginal projections.

Lastly, we recorded a spectrum of higher order modes to compare the distance between modes with Equation (6). Again, the data with calibrated x-Axis and fitted lorentzians can be seen in Figure 9.

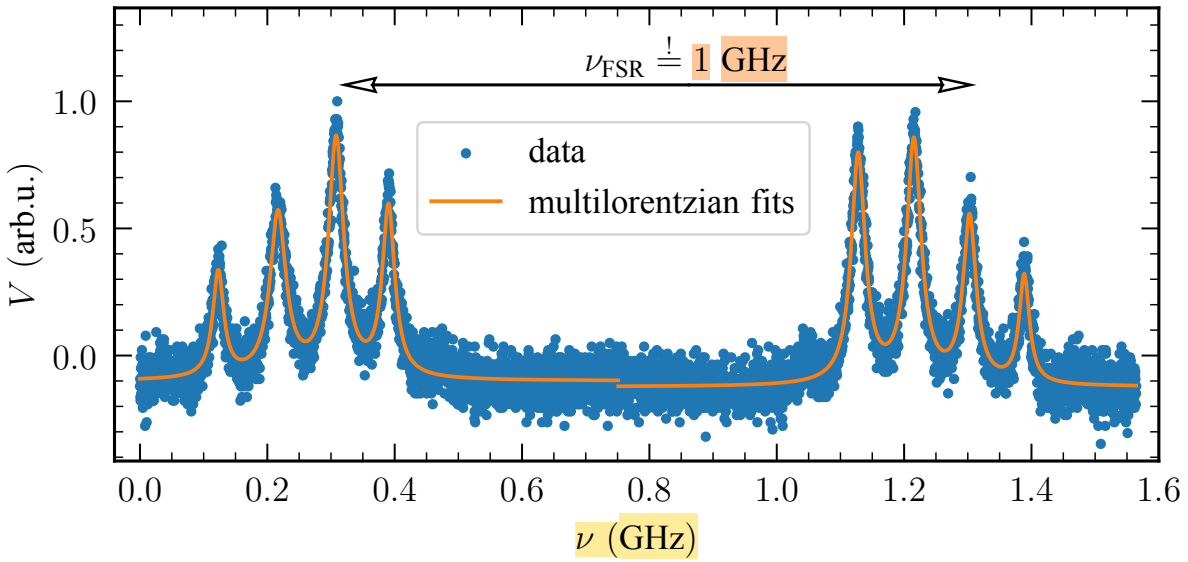

Figure 9: The recorded signal amplitude V is plotted against the frequency ν. The data was split in equal halves, to which functions consisting of four independent Lorentz functions were fitted and can be seen as solid orange lines. The distance between the third peaks from the left was used to calibrate the x-Axis, while the distance to the half axial peak, seen in the middle was determined from fit parameters.

From the fits, we get a mean mode spacing of $\Delta\nu = 88.03(8)$ MHz. From the theory side, replacing the mirror spacing $L = 150$ mm in confocal setup with the new length of $L = 163.53(1)$ mm, $\arccos(1 - L/r)/\pi$ increases from exactly 0.5 to 0.529(2). This leads to a shift in frequency for higher modes (m,$n > 0$) with increasing q, as can be seen in Figure 2. However, the predicted fundamental mode spacing of 29(2) MHz is too small to explain the data. Only moving to modes with $m+n = 2$ (this effectively rescales the output of the arccos), the predicted mode spacing becomes 86(6) MHz. Whilst in good agreeance with experimental results, it requires dominant TEM_{mn} modes with $m + n = 2$. Although possible, it is quite unlikely that we do not simultaneously excite higher or lower modes. It is also possible, that we did not observe a full FSR of the cavity with the recorded data still representing substructures, rendering our x-Axis calibration false.

4 Interpretation

We successfully determined the HeNe laser's beam waist to $w_0 = 224(2)$ µm, with data following the predicted behavior. When adding a lens, again the theoretically calculated value $w_{1,\mathrm{theo}} = 83.3(1.1)$ µm and the experimental $w_{1,\mathrm{exp}} = 82(3)$ µm are consistent with each other. Here, the datapoints deviated somewhat from the expected line, which can probably be traced back to inaccuracies in the measurement setup. Mounting the waistmeter on a movable rail would aid in keeping the waistmeter orthogonal to the incident laser beam, which is paramount for accurate readings.

After simulating and successfully matching the laser beam to the cavity's internal modes, we validated the cavity to be confocal by measuring the distance between "regular" and half axial

modes. Next, we fine-tuned the mirrors to reduce the half axial mode's intensity and determined the finesse of the cavity $\mathcal{F}_{\text{exp}} = 75.91(15)$ by fitting Lorentz functions to a recorded spectrum. Assuming all resonator losses to stem from a mirror reflectivity of 98%, we calculated an upper limit of $\mathcal{F}_{\text{theo}} = 155.50$. Clearly, other losses are present in the system, such as absorption on dust particles. Also, mirrors degrade with time, reducing their reflectivity.

Leaving the confocal condition, we observe higher mode excitations. We can correctly identify TEM_{00}, TEM_{01} and TEM_{10} modes taking an optical image with a CCD camera and fitting Hermite-Gaussian polynomials to projected intensities. We also took a picture of what could be a TEM_{02} mode, however it is vertically not completely contained in the image, so a definitive identification is difficult. Two of the four pictures show saturation of the CCD intensity, which could be remedied by using a filter.

Lastly, we determined the mode spacing of higher modes by fitting Lorentz functions to a recorded spectrum. We measure it to be $\Delta\nu = 88.03(8)$ MHz. We can theoretically explain this result assuming the only excited TEM_{mn} modes satisfy $m + n = 2$, which is highly unlikely. Another possibility is that we did not capture a full spectral range of the cavity, falsifying our conversion from time to frequency domain.

References

[1] *Gaussian beams and optical resonators*. Universität Innsbruck, Innsbruck, AT: Institut für Experimentalphysik, 2024.

[2] *Practical course experiment 09: Diodelaser*. Universität Innsbruck, Innsbruck, AT: Institut für Experimentalphysik, Dec. 2024.

[3] THORLABS. *Fabry-Perot Interferometer Tutorial*. Online; Abgerufen am 21. 03. 2024. URL: https://www.thorlabs.com/newgrouppage9.cfm?objectgroup_id=9021.

[4] Wikipedia contributors. *Optical cavity — Wikipedia, The Free Encyclopedia*. [Online; accessed 10-April-2024]. 2024. URL: https://en.wikipedia.org/w/index.php?title=Optical_cavity&oldid=1194071668.

[5] *Lightmachinery*. Online; accessed at April 10, 2024. URL: https://lightmachinery.com/optical-design-center/gaussian-beam-propagation/?gad_source=1.

Erklärung

Hiermit versichern wir, dass der vorliegende Bericht selbständig verfasst wurde und alle notwendigen Quellen und Referenzen angegeben sind.

April 15, 2024

Alexander Helbok — Date

April 15, 2024

Jakob Hugo Höck — Date

April 15, 2024

Max Koppelstätter — Date